

Modeling the amplification of epidemic spread by misinformed populations

Matthew R. DeVerna^{1,†}, Francesco Pierri², Yong-Yeol Ahn¹, Santo Fortunato¹, Alessandro Flammini¹, and Filippo Menczer¹

¹*Luddy School of Informatics, Computing, and Engineering, Indiana University, Bloomington, USA*

²*Department of Electronics, Information and Bioengineering, Politecnico di Milano, Milano, Italy*

[†]*Corresponding author. Email: mdeverna@iu.edu*

This preprint has not yet undergone peer review.

July 31, 2024

Abstract

Understanding how misinformation affects the spread of disease is crucial for public health, especially given recent research indicating that misinformation can increase vaccine hesitancy and discourage vaccine uptake. However, it is difficult to investigate the interaction between misinformation and epidemic outcomes due to the dearth of data-informed holistic epidemic models. Here, we employ an epidemic model that incorporates a large, mobility-informed physical contact network as well as the distribution of misinformed individuals across counties derived from social media data. The model allows us to simulate and estimate various scenarios to understand the impact of misinformation on epidemic spreading. Using this model, we present a worst-case scenario in which a heavily misinformed population would result in an additional 14% of the U.S. population becoming infected over the course of the COVID-19 epidemic, compared to a best-case scenario.

Social factors, such as information sharing, play a crucial role in shaping the dynamics and epidemiology of infectious diseases^{12,5}. For instance, a population’s willingness to adopt public health measures (or lack thereof) largely determines their successes or failures^{34,4}. A population’s behavioral response to outbreaks can be influenced by mass media, as witnessed during the 2009 H1N1 influenza pandemic⁴⁰, or by social media and the anti-vaccination movement^{1,26,10,13}.

A great deal of work has explored how to model the influence of human behaviour on the spread of infectious diseases^{53,25}. Here we focus on risky behaviors affecting disease transmission that are associated with misinformed individuals. Misinformation spreading on social networks has been linked to poor compliance with COVID-19 public health guidance⁴⁵. Greater exposure to unreliable news articles about COVID-19 vaccines has been linked to an increase in vaccine hesitancy and a decrease in vaccination rates at both state and county levels in the United States^{42,39}. Exposure to online misinformation has also been shown to increase vaccine hesitancy in laboratory experiments³³. This is particularly detrimental during vaccination campaigns as clusters of individuals adopting anti-vaccination opinions can make it challenging for a population to reach herd immunity^{17,47}. Proper management of epidemic crises in the modern age thus requires the understanding of the complex relationship between the spread of (mis)information through online social networks and the spread of disease through physical contact networks (Fig. 1).

While previous agent-based simulations have shown that misinformation may impede the suppression of epidemics in various ways^{50,36,41,9}, there is a growing need to integrate real-world data to strengthen the connections between simulation results and real-world outcomes. Social media can provide valuable data sources for this purpose^{6,51}.

We address this challenge by proposing a data-informed epidemic model that takes both the distribution of misinformed individuals and a physical mobility network into account. Using this data, we augment the Susceptible-Infected-Recovered (SIR) model to account for a subpopulation of “misinformed” individuals. We explore how this group can affect the larger, ordinary population using both a mean-field approximation, which assumes all individuals have an equal chance of interacting, and a multi-level agent-based simulation based on two large, data-informed networks: a social network where misinformation spreads and a contact network where the disease can propagate. A contact network of approximately 20 million nodes is constructed by leveraging large-scale Twitter data, county-level voting records, and cellphone mobility data. We incorporate theoretically extreme values of the parameter responsible for the epidemic transmission to evaluate best- and worst-case scenarios about the impact of misinformed individuals on the spread of disease and obtain quantitative bounds on the harm caused by misinformation.

Results

In our model, as in the standard SIR modeling framework², a parameter β describes the average number of infected individuals generated by an infected individual in a time unit. Infected individuals recover with

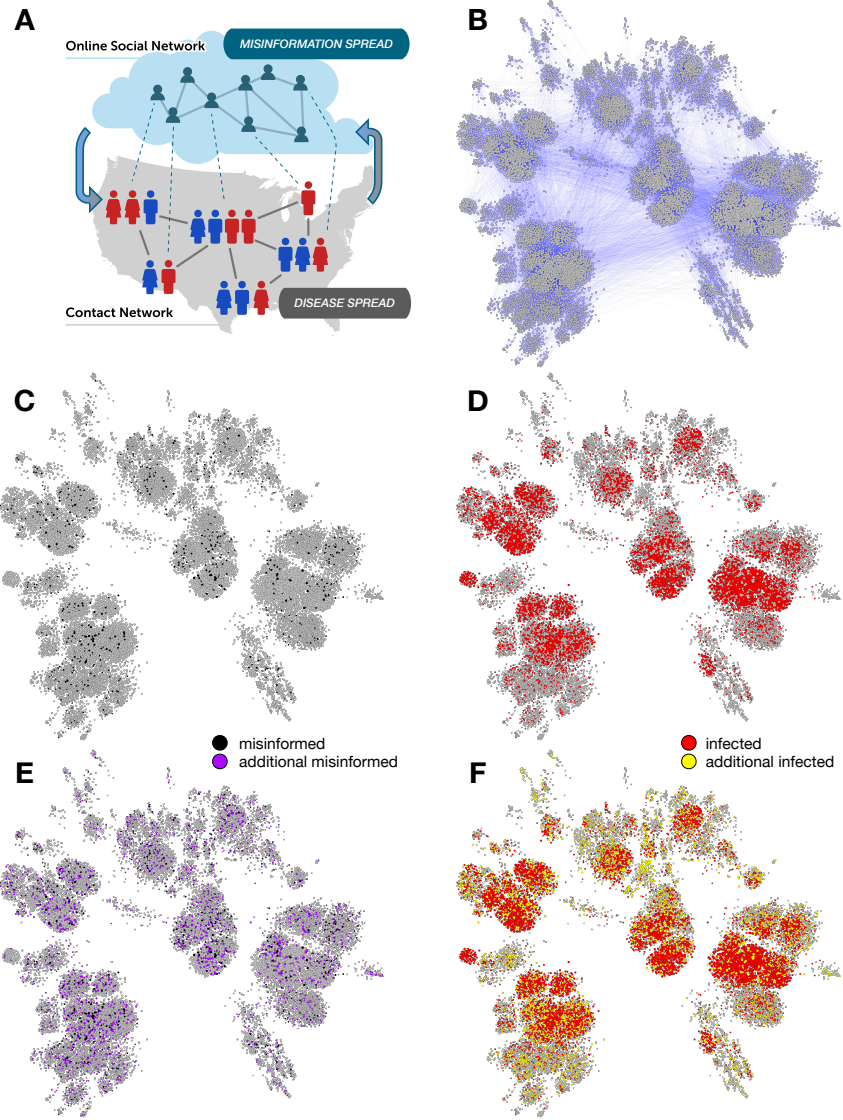


Figure 1: The spread of misinformation affects the transmission of disease. (A) Schematic illustration of the misinformation and contact networks. Online social networks foster misinformation dissemination while physical contact networks, such as those that connect co-workers in an office or pupils in a school, facilitate disease transmission. Dotted links indicate that the same people participate in both networks, which have different topologies; e.g., the information network tends to have stronger political homophily while the contact network tends to have stronger geographic homophily. We focus on the impact of misinformation spread on disease transmission (downward arrow), while the opposite effect (upward arrow, e.g., individuals ceasing to share misinformation due to illness) falls outside the scope of this investigation. (B) A contact network based on 0.01% county population samples. Nodes are sized based on degree (number of contacts). In a scenario with limited spread of misinformation (black nodes in C), the simulations of disease spread leads to a number of infected individuals (red nodes in D). In a scenario where the misinformation spreads more widely (purple nodes in E), more individuals get infected (yellow nodes in F).

rate γ . We extend this epidemic model to account for misinformed and ordinary subpopulations. We utilize six compartments to capture the three stages of SIR for each subpopulation. The fractions of individuals in the susceptible, infected, and recovered compartments are denoted by S_O , I_O , and R_O respectively for the ordinary group; and by S_M , I_M , and R_M for the misinformed group.

Ordinary individuals are considered to be well-informed about public health guidelines, while misinformed individuals, having been exposed to untrustworthy information, are assumed to be less likely to follow recommended behaviors, such as social distancing, mask-wearing, and vaccination, thereby increasing the risk of infection for themselves and others²⁰. We therefore define two distinct parameters β_O and β_M for ordinary and misinformed susceptibles, respectively. We model the risky behavior of the misinformed group by setting $\beta_M \geq \beta_O$. The recovery rate γ is identical for both subpopulations. We refer to this as the Susceptible Misinformed Infected Recovered (SMIR) model.

Mean-field simulations

The mean-field approach assumes that an infected individual can transmit disease to *any* susceptible individual. With this assumption, we derive the model’s mean-field system of equations (see Methods) and explore parameter values for which epidemic spread occurs. We denote the proportions of ordinary and misinformed individuals as μ and $1 - \mu$, respectively. An initial proportion of the population ϵ is infected, split evenly between the ordinary and misinformed groups. Thus, we initialize the compartments with $I_O = \frac{\epsilon}{2}$, $I_M = \frac{\epsilon}{2}$, $S_O = \mu - \frac{\epsilon}{2}$, $S_M = 1 - \mu - \frac{\epsilon}{2}$, and $R_O = R_M = 0$.

The effects of varying the transmission and recovery parameters are predictable (see Supplementary Information): lower β and higher γ “flatten the curve” and reduce the negative outcomes of an infection. Based on these explorations we set $\beta_O = 0.3$ and $\gamma = 0.2$ such that the basic reproduction number $R_0 = \beta/\gamma > 1$ to ensure epidemic spread. Next we focus on the effects of varying the misinformed subpopulation’s level of risk and the degree of homophily within the network.

To explore the effects of risky behaviors by misinformed individuals, let us assume two equally-sized subpopulations ($\mu = 1/2$) and introduce the scaling factor $\lambda = \beta_M/\beta_O \geq 1$. Fig. 2 illustrates the increasing negative impact of the misinformed subpopulation on the disease-spreading dynamics as λ becomes larger. The social cost associated with the more risky behaviors by the misinformed group is passed on to the whole network. For example, when $\lambda = 3.0$, peak infection for the entire population is reached 38 days earlier than in the $\lambda = 1$ case (day 22 vs. 60; Fig. 2A), leading to an additional 29.2% of the population becoming infected (Fig. 2B).

Let us explore the effect of homophily among the ordinary and misinformed subpopulation networks. Homophily means that infected individuals are more likely to interact with (and infect) susceptibles from the same subpopulation (ordinary or misinformed) than the other group. The degree of homophily is modeled by a parameter α . When $\alpha = 0.5$, individuals are equally likely to interact within and across groups (no homophily), whereas $\alpha = 1$ is the case when homophily is strongest and the subpopulations do not interact

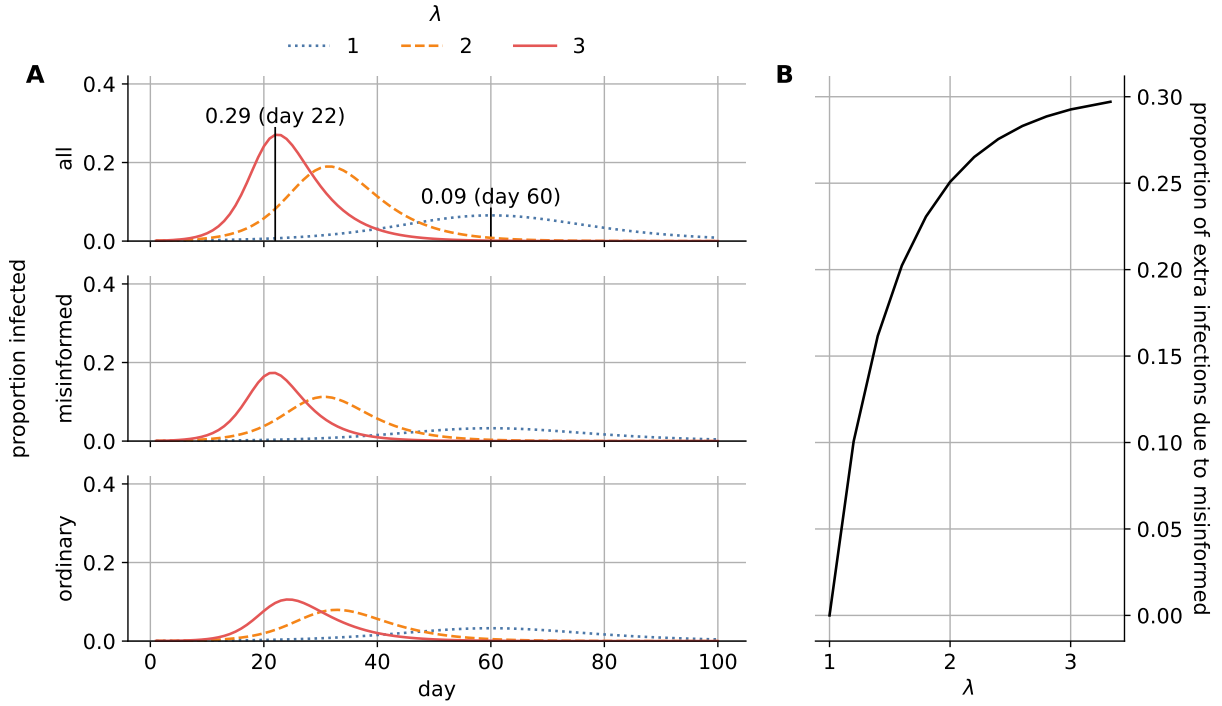


Figure 2: Increasing $\lambda = \beta_M/\beta_O$ accelerates and amplifies the infection. We use $\beta_O = 0.3$, $\gamma = 0.2$, and $\mu = 0.5$. (A) Proportion of the population infected on each day. (B) Extra proportion of the total population that is infected as a function of λ .

with each other (see Methods for details).

Fig. 3 illustrates the effects of homophily ($0.5 \leq \alpha \leq 1$) for different levels of ordinary transmission ($0.1 \leq \beta_O \leq 0.4$). For less infectious disease (low β_O), increasing homophily significantly harms the misinformed group (Fig. 3B): the infection remains confined within this group. There is no discernible effect on the ordinary population as long as the two groups interact; when they do not ($\alpha = 1$), we observe a sharp reduction in infections (Fig. 3A). For $0.12 < \beta_O < 0.16$, peak infection scenarios coincide with intermediate homophily levels, as indicated by the black dots in Fig. 3C³⁷. Under these conditions, while increased homophily decreases infections in the general populace, it significantly worsens outcomes for the misinformed group (compare Fig. 3B and C). As β_O increases further, while nearly the entire misinformed population becomes infected regardless of α (Fig. 3B), high homophily shields the full population (Fig. 3C): ordinary individuals have a lower risk of becoming infected through interactions with misinformed individuals. In summary, homophily offers greater protection to the ordinary group by isolating misinformed communities, which suffer a greater disease burden, exacerbating health disparities^{46,49}.

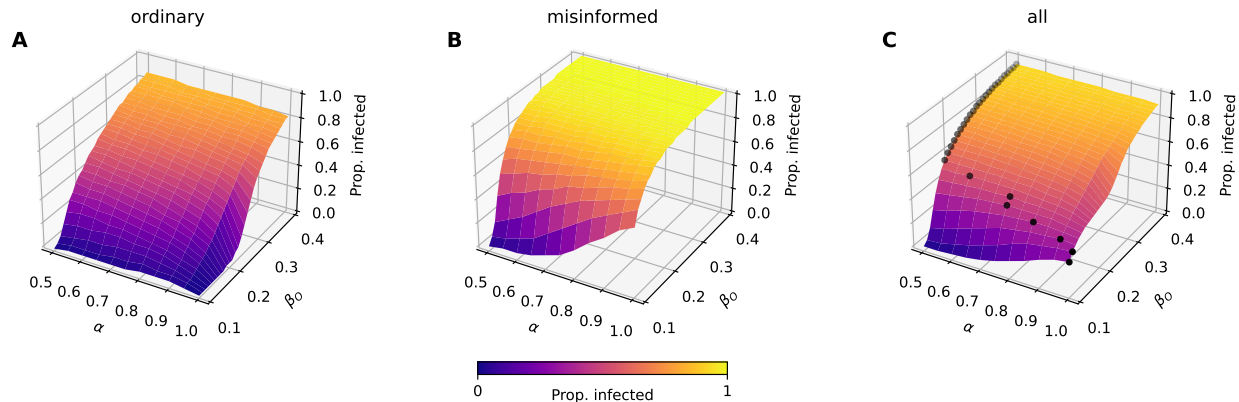


Figure 3: Homophily in the contact network worsens the infection among misinformed individuals, especially for lower transmission rates. The combined effects of transmission and homophily parameters, β_O and α , are examined with the mean-field approximation when $\lambda = 3$, $\gamma = 0.2$, and $\mu = 0.5$. We plot the proportions of infected individuals in (A) the ordinary population, (B) the misinformed population, and (C) the overall population. The maximum proportion of the overall population infected for each β_O is marked with a black dot. When the transmission rate is sufficiently high, homophily benefits the entire population but harms the misinformed group.

Agent-based simulations

To examine the influence of misinformation within a more realistic epidemic framework, we utilize a multi-level model. Our approach combines an empirically derived information network with a contact network calibrated with real-world data, as illustrated in Fig. 4. Information diffusion is modeled by leveraging a large set of users of a popular social media platform and epidemic simulations are subsequently conducted on contact networks populated with misinformed individuals.

We leverage a large collection of English-language discussions taking place on Twitter about COVID-19 vaccines²². From approximately nine months of this data (Jan. 4–Sep. 30, 2021), we geolocate over 2 million U.S. users who shared almost 26 million tweets and focus on accounts in 341 U.S. counties containing more than 200 Twitter users each. We also infer an account’s political alignment and whether they shared any likely misinformation (see Methods). Twitter is not representative of the U.S. population, and people also access information in other ways, such as traditional media and word of mouth. However, this empirical social network serves as a data-informed proxy for a large, realistic network through which people share information about the disease.

With this data, we build a directed and weighted information diffusion network, in which an edge ($i \rightarrow j, w$) indicates that j retweeted i w times. There are various ways to model the infodemic¹⁹. We simulate the spread of misinformation on this network, as illustrated in Fig. 4A. Accounts that share or reshare posts containing misinformation are considered misinformed. These accounts function as the initial *seeds* from which misinformation proliferates to the wider network. Not all users actively participate in content sharing, with only about half of U.S. Twitter users, for instance, engaging in this activity³⁸. But even without active

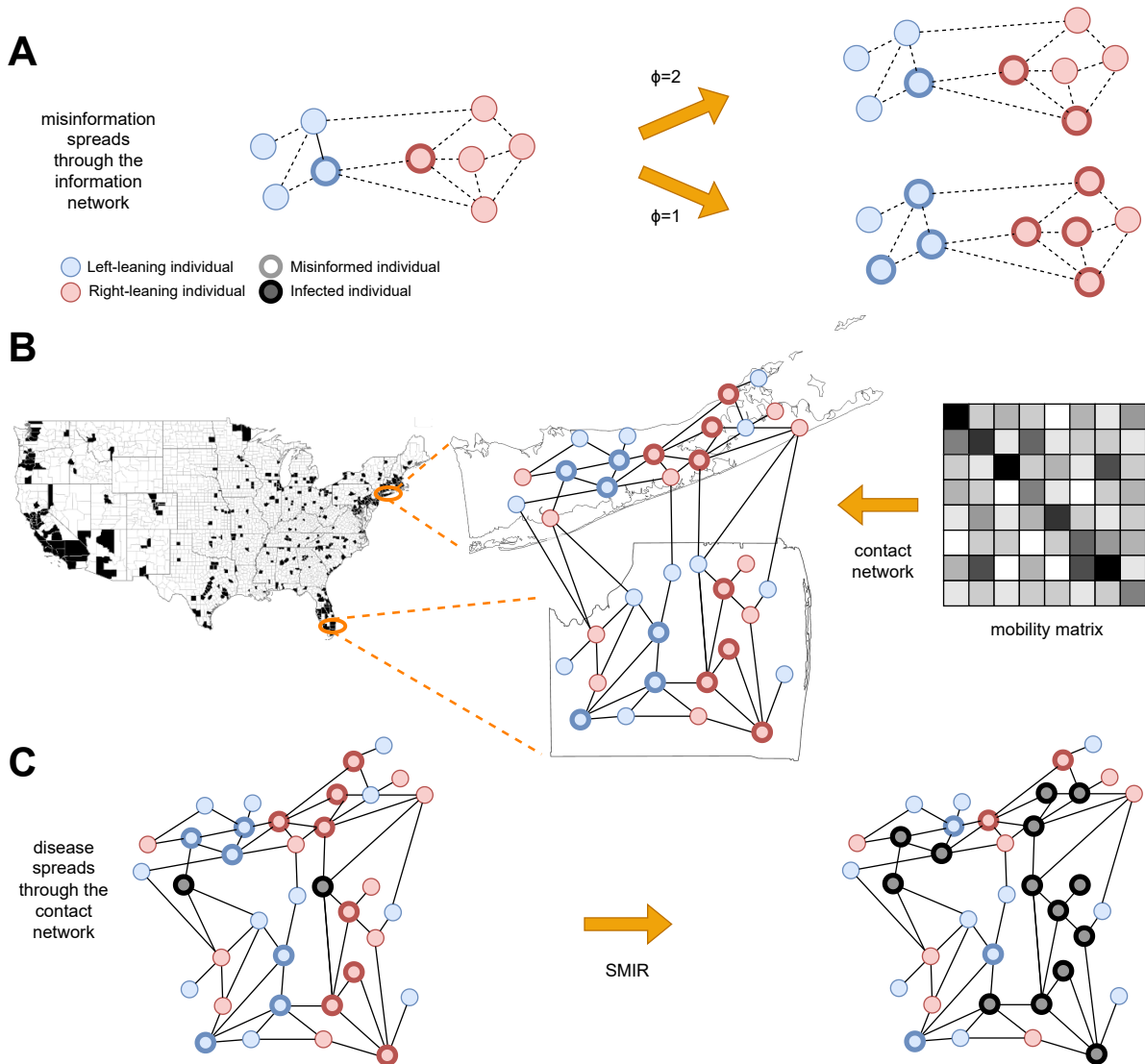


Figure 4: An idealized example of our multi-level modeling framework. **(A)** Spread of misinformation through an information network (dashed lines). Colors represent ideological homophily. Nodes with bold borders are misinformed about the epidemic. The misinformation spreads through a complex contagion (linear threshold) model; two scenarios show that a lower threshold ϕ leads to more misinformed nodes. **(B)** Construction of the contact network (solid lines) for counties with sufficient information diffusion data (in black) to provide reasonable estimates about the fraction of misinformed individuals. Note that these counties account for 63.52% of U.S. voters. Each location's population size and ideological mix are based on empirical data, and misinformed individuals are based on the information diffusion model. Links among individuals within and between locations are based on empirical mobility data. **(C)** The infection spreads through the contact network (black nodes), according to the SMIR model.

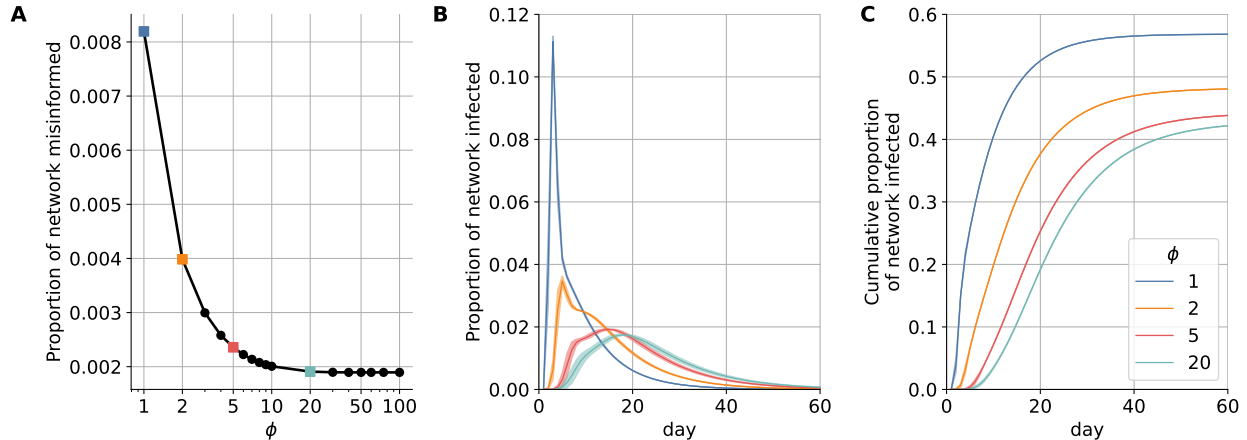


Figure 5: More misinformed individuals lead to a larger portion of the network becoming infected. Decreasing the resilience ϕ (A) increases the size of the misinformed subpopulation, leading to (B) faster infection spreading and (C) a greater cumulative number of infections. In panels (B, C), lines and corresponding shaded regions represent the mean and standard deviation across simulations, respectively.

sharing, exposure to misinformation can still influence individual behavior³³.

To account for users who may be misinformed through exposure, we employ a single-step linear threshold opinion-spreading process²⁷. While many social influence models have been proposed¹⁴, this is a simple way to capture complex contagion, according to which individuals require multiple exposures to misinformation before they become misinformed themselves^{16,54,35}. Let a linear threshold ϕ represent the minimum number of misinformed friends needed for an ordinary node to become misinformed. If the total number of misinformed friends of i is greater than or equal to ϕ , i is marked as misinformed (M). The remaining nodes are marked as ordinary susceptibles (O). We can interpret ϕ as a measure of “resilience” to misinformation; as it increases, individuals require more exposure to misinformation to be converted to the misinformed group. Note that since we explore the full range of ϕ values, the following results are unaffected whether the threshold is defined based on the number of users or the number of retweets.

Fig. 5A shows how ϕ influences the number of misinformed individuals within the retweet network. With strong resilience ($\phi > 10$), exposure to misinformation does not have much effect and few nodes are converted to the misinformed group. Conversely, when resilience to misinformation is very low (as in the simple contagion case $\phi = 1$), all nodes exposed to a misinformation-containing post are converted to the misinformed group. Through this process, empirically observed misinformation-sharing behavior leads to information networks with misinformed subpopulations of varying sizes based on different ϕ values.

We generate contact networks for different thresholds ($1 \leq \phi \leq 20$) to compare the impact of misinformed subpopulations of different sizes. Given a threshold ϕ and the corresponding information network, we aim to construct a physical contact network containing empirically calibrated misinformed subpopulations (Fig. 4B). The process begins by selecting a sample of individuals from each county within the information

network. As party affiliation has been identified as a risk factor associated with excess mortality during the COVID-19 pandemic²⁹, county samples are constructed to match the percentage of Republicans and Democrats who voted in the 2020 U.S. presidential election. For each county, we add the sampled nodes to the physical network marked as misinformed (M) or ordinary susceptible (O), based on their label within the retweet network. Sampling with replacement allows us to select individuals such that the overall proportions of Republicans and Democrats match the voting records. A 10% sample leads to $N \approx 20$ million nodes. A network based on a much smaller sample is illustrated in Fig. 1B. This process captures empirical measurements of the ideological split, relative population size, and quantity of misinformed individuals in each county. We add contact network edges by leveraging cell phone mobility data that provides the probability of an individual traveling within and between counties. See Methods for details.

Disease-spreading dynamics on a contact network are simulated using an agent-based version of SMIR (Fig. 4C). Two critical parameters affecting these dynamics are the density of the contact network, captured by its average degree \bar{k} , and the transmission probability p (note that $p\bar{k} = \beta$). Mitigation measures such as social distancing decrease \bar{k} , while those such as masking and vaccination decrease p . A simple way to model the combined effects of misinformation on these behaviors is to set $\bar{k} = 25$, a high value corresponding to the average number of daily contacts prior to the COVID-19 pandemic³², and explore a wide range of transmission probabilities to capture worst- and best-case scenarios. To this end, we model the refusal of any mitigation measures by selecting the maximum value $p_M = 1$ for misinformed individuals. In contrast, we model the adoption of several mitigation measures by selecting an extremely small value $p_O = 0.01$ for ordinary individuals. These values illustrate two theoretically extreme scenarios. The former portrays a realistic number of interactions during non-pandemic times, accompanied by high transmission rates due to the absence of preventive measures, such as social distancing, mask-wearing, or vaccinations. The latter demonstrates decreased daily interactions and reduced transmission rates resulting from the implementation of these preventive measures. Using the empirically calibrated contact networks in conjunction with these extreme parameters, the simulation approach allows us to bound the best- and worst-case scenarios in a data-informed manner (see Methods for more information).

The worst-case effect of the misinformed subpopulation size on the daily incidence of infection (illustrated in Fig. 1C-F on a small network) is quantified in Fig. 5B on a large network (10% sample). A heavily misinformed population ($\phi = 1$) corresponds to an additional 9% of the population being infected at peak time (a six-fold increase) compared to a population following expert guidance in the best-case scenario ($\phi = 20$). The peak also occurs approximately two weeks earlier. The cumulative effect of a heavily misinformed population is also significant, with an additional 14% of the population infected over the course of the epidemic — a 32% relative increase (Fig. 5C). We repeated this analysis for different sample sizes and found that the main results are robust (see Supplementary Information).

Discussion

This work presents large-scale simulations based on an epidemic model that accounts for a subpopulation of misinformed individuals, informed by real-world data. Such an approach answers calls from the literature to anchor models in empirical data^{6,51}, allowing us to explore realistic potential outcomes. While we know that exposure to online health misinformation is associated with risky behaviors such as vaccine hesitancy and refusal³⁹, our model further links these behaviors by a misinformed population to an accelerated spread of disease.

By deriving the mean-field system of equations for the novel SMIR model and exploring its dynamics, we demonstrate how the risky behaviors of misinformed individuals can adversely impact those following public health guidelines, worsening outcomes for the entire population. Additionally, increasing homophily can benefit the overall population by protecting ordinary citizens; however, it may also lead to higher infection rates within the misinformed subpopulation.

Agent-based simulations of the SMIR model let us study the epidemic on empirically calibrated contact networks, which provide more realistic scenarios compared to the mean-field approach. The model estimates that, in the worst-case scenario, a heavily misinformed population can amplify the peak of the infection by a factor of six and accelerate it by two weeks. This would result in an additional 14% of the population becoming infected — nearly 47 million Americans based on recent U.S. Census data⁵². The corresponding price tag of vaccine misinformation would be over \$143B, using estimated health care costs associated with COVID-19 in the U.S.³.

While these figures are based on extreme scenarios, they represent an alarming bound on the harm of exposure to online vaccine misinformation. They should provide public health authorities as well as social media platforms with heightened motivation to curb vaccine misinformation, despite the difficulties posed by social media design¹¹.

We acknowledge certain limitations in our approach. While individual beliefs and behaviors may vary over time, our model simplifies the scenario by dichotomizing individuals into misinformed and ordinary subpopulations and assuming constant transmission rates. We also assume uniform resilience to misinformation for all individuals during the information diffusion process, although this attribute likely differs across individuals. Future directions could involve more sophisticated models to account for these heterogeneities. For instance, cognitive models of misinformation acceptance⁷ could be incorporated into the simulation with misinformation exposure data collected from social media. Such integration would enable the transition of individuals from ordinary to misinformed susceptible states throughout the simulation, allowing for a simultaneous examination of opinion and disease dynamics. Some theoretical models have already explored similar approaches and obtained results that align with our findings^{36,50}.

Future work should attempt to analyze the potential effects of misinformation in more realistic scenarios, where values for the key parameters p_M and p_O could be obtained by calibrating the model with empirical epidemic data from particular regions and time periods. Additional extensions of the model could account

for a feedback loop whereby witnessing local infections could drive changes in behaviors equivalent to the transition of individuals out of the misinformed population.

Methods

SMIR model. For both the ordinary and misinformed subpopulations, the Susceptible Misinformed Infected Recovered (SMIR) model replicates the standard SIR compartments, denoted as $S_O/I_O/R_O$ and $S_M/I_M/R_M$, respectively. While SMIR adopts distinct transmission parameters for the misinformed and ordinary groups (β_M and β_O , respectively), the mean-field approach assumes that infected individuals from either group ($I_O + I_M$) can potentially infect *anyone* in the susceptible populations. The mean-field model is governed by the following system of equations:

$$\begin{cases} \frac{dS_O}{dt} = -\beta_O S_O (I_O + I_M), & \frac{dI_O}{dt} = \beta_O S_O (I_O + I_M) - \gamma I_O, & \frac{dR_O}{dt} = \gamma I_O \\ \frac{dS_M}{dt} = -\beta_M S_M (I_O + I_M), & \frac{dI_M}{dt} = \beta_M S_M (I_O + I_M) - \gamma I_M, & \frac{dR_M}{dt} = \gamma I_M. \end{cases} \quad (1)$$

To account for homophily, we modify the term $I_O + I_M$ in Eq. 1 to account for increased (decreased) contacts within (across) groups, according to the parameter $\alpha \geq 0.5$. When homophily does not play a role ($\alpha = 0.5$), there is an equal probability of interacting with either subpopulation’s infected group. We thus obtain:

$$\begin{cases} \frac{dS_O}{dt} = -2\beta_O S_O (I_O \alpha + I_M (1 - \alpha)), & \frac{dI_O}{dt} = 2\beta_O S_O (I_O \alpha + I_M (1 - \alpha)) - \gamma I_O, & \frac{dR_O}{dt} = \gamma I_O \\ \frac{dS_M}{dt} = -2\beta_M S_M (I_O (1 - \alpha) + I_M \alpha), & \frac{dI_M}{dt} = 2\beta_M S_M (I_O (1 - \alpha) + I_M \alpha) - \gamma I_M, & \frac{dR_M}{dt} = \gamma I_M. \end{cases} \quad (2)$$

We initialize the simulation by randomly marking $\frac{\epsilon}{2}$ nodes as infected in both the misinformed and ordinary groups, where $\epsilon = 0.001$.

Twitter and derived data. Twitter posts in the CoVaxxy dataset²² were collected in real time via the stream/filter endpoint of the Twitter Application Programming Interface (API). To capture the online discourse surrounding COVID-19 vaccines in English, a comprehensive set of English-language keywords was carefully curated. Beginning with the initial seeds of “covid” and “vaccine,” a snowball sampling technique²³ was used to identify co-occurring relevant keywords in December 2020²². The resulting list contained almost 80 keywords, available online²¹. To confirm the relevance of the collected tweets to the topic of vaccines, we examined the coverage obtained by incrementally adding keywords, starting with the most common ones. Over 90% of the tweets in 2021 contained at least one of the three most common keywords: “vaccine,” “vaccination,” or “vaccinate.” To infer the location of accounts, we used the Carmen Python library²⁴ that leverages self-reported location metadata within user profiles (embedded in tweets). As an account’s location may change over time (captured across multiple tweets), we utilize the most recent location. We geolocate 2,047,800 users residing in all 50 U.S. states, who shared a total of 25,806,856 tweets by mapping self-reported locations to U.S. counties. The information network is constructed from accounts in 341 counties that contain more than 200 Twitter users each. Political alignment is estimated using a third-party list of annotated news

sources^{44,43}. It is averaged across all the sources shared by each account. Nodes with an estimated alignment greater (smaller) than zero are considered Republican (Democrat). We infer the political alignment of some additional accounts, who did not share links to news sources, using a label-propagation algorithm¹⁸ on the retweet network. If all of a node’s neighbors have political alignment scores, its score is estimated using the weighted average of its neighbors, with weights based on retweets. The process is iterated until each node without a score has at least one neighbor without a score. Misinformation is defined at the source level. Tweets containing links to articles from a list of low-credibility sources compiled by NewsGuard (score below 60) are labeled as spreading misinformation. This approach is common practice and has been validated in the literature^{39,28,8,31,48}.

Contact network edges. To construct edges in our contact network, we utilize SafeGraph cell-phone mobility data⁵⁵, which contains information on the number of people residing in over 200K Census-Block-Groups (CBG) who visited 4.3M Points-of-Interest (POI) in the United States. This data has been widely employed to study human mobility patterns during the COVID pandemic. We used the average daily number of individuals moving during 2019, as a reference for business-as-usual mobility, and aggregated all CBGs and POIs at the county level. This aggregation results in a county-by-county matrix L , where each element L_{xy} represents the average daily number of individuals in county x moving to county y or vice versa. We then normalized L_{xy} to obtain the average probability of individuals in counties x and y coming into contact, and multiplied by the total number of edges to obtain the expected number of connections between individuals in counties x and y : $E_{xy} = \frac{L_{xy}}{\sum_{x',y'} L_{x'y'}} \frac{\bar{k}N}{2}$ where the sum is over all county pairs and $\frac{\bar{k}N}{2}$ is the total number of edges. Next, we create a physical contact network with N nodes by following a procedure akin to a stochastic block model³⁰ used to generate networks with localized communities. For each pair of distinct locations x and y , we draw E_{xy} edges between random pairs of nodes in x and y . Additionally, we draw E_{xx} edges among random pairs of individuals within the same location x , representing homogeneous mixing within each county. At the end of the process, the network has the target average degree \bar{k} . We use $\bar{k} = 25$ and show how this parameter affects the infections in Supplementary Information.

Simulation details. Agent-based SMIR simulations are initiated by randomly selecting 100 misinformed nodes and designating them as infected. The disease spreading dynamics are then simulated for 100 steps, which correspond to days. To align with COVID-19 dynamics, we utilize the CDC’s recommended quarantine period of 5 days as our recovery period¹⁵ ($\gamma = 0.2$). Each simulation is repeated ten times, and the average outcome is reported.

Data and code availability. Code and data are available in a public repository ([github.iu.edu/NaN-team/bounding-misinfo-impact-on-disease-spread](https://github.com/NaN-team/bounding-misinfo-impact-on-disease-spread)).

Acknowledgments

We are grateful to Yuan Yuan, Marco Ajelli, Alessio Brina, and Brea Perry for helpful discussions. This work was supported in part by the Swiss National Science Foundation (grant 209250), the National Science Foundation (grants 1927425 and 1927418), the Army Research Office (contract W911NF-21-1-0194), the European Union (NextGenerationEU project PNR-PE-AI FAIR), the Italian Ministry of Education (PRIN PNR grant CODE prot. P2022AKRZ9 and PRIN grant DEMON prot. 2022BAXSPY), Knight Foundation, and Craig Newmark Philanthropies.

Author contributions

The initial concept for this research was developed by YA, SF, AF, FM. The final study design was developed collectively by all authors. Data collection was led by MRD as part of the CoVaxxy project²¹. All mean-field modeling was conducted by MRD. FP developed the early code for the agent-based simulation, which was subsequently refined and expanded by MRD for publication. Analysis was conducted primarily by MRD, with help from FP, and guidance from YA, SF, AF, FM. The SMIR model was developed collaboratively by all authors. Visualizations were created by MRD, FP, and FM with input from all authors. The first draft was written by MRD, with revisions from all authors. FM oversaw the progression of the study.

Competing interests

Authors declare that they have no competing interests.

Ethics

This study, focusing on public data, poses minimal risk to human subjects. Consequently, the Indiana University Institutional Review Board has exempted it from review (protocol number 1102004860). All data collection and analysis adhered to Twitter's terms of service.

References

- [1] J. N. L. Allen, D. J. Watts, and D. Rand. Quantifying the Impact of Misinformation and Vaccine-Skeptical Content on Facebook. *PsyArXiv*, Oct. 2023. URL <https://doi.org/10.31234/osf.io/nwsqa>.
- [2] R. M. Anderson and R. M. May. *Infectious diseases of humans: dynamics and control*. Oxford university press, 1991.

- [3] S. M. Bartsch, M. C. Ferguson, J. A. McKinnell, K. J. O’Shea, P. T. Wedlock, S. S. Siegmund, and B. Y. Lee. The Potential Health Care Costs And Resource Use Associated With COVID-19 In The United States. *Health Affairs*, 39(6):927–935, 2020. doi: 10.1377/hlthaff.2020.00426. URL <https://doi.org/10.1377/hlthaff.2020.00426>.
- [4] C. T. Bauch and A. P. Galvani. Social Factors in Epidemiology. *Science*, 342(6154):47–49, Oct. 2013. URL <https://doi.org/10.1126/science.1244492>.
- [5] J. J. V. Bavel, K. Baicker, P. S. Boggio, V. Capraro, A. Cichocka, M. Cikara, M. J. Crockett, A. J. Crum, K. M. Douglas, J. N. Druckman, J. Drury, O. Dube, N. Ellemers, E. J. Finkel, J. H. Fowler, M. Gelfand, S. Han, S. A. Haslam, J. Jetten, S. Kitayama, D. Mobbs, L. E. Napper, D. J. Packer, G. Pennycook, E. Peters, R. E. Petty, D. G. Rand, S. D. Reicher, S. Schnall, A. Shariff, L. J. Skitka, S. S. Smith, C. R. Sunstein, N. Tabri, J. A. Tucker, S. v. d. Linden, P. v. Lange, K. A. Weeden, M. J. A. Wohl, J. Zaki, S. R. Zion, and R. Willer. Using social and behavioural science to support COVID-19 pandemic response. *Nat Hum Behav*, 4:460–471, May 2020. URL <https://doi.org/10.1038/s41562-020-0884-z>.
- [6] J. Bedson, L. A. Skrip, D. Pedi, S. Abramowitz, S. Carter, M. F. Jalloh, S. Funk, N. Gobat, T. Giles-Vernick, G. Chowell, J. R. de Almeida, R. Elessawi, S. V. Scarpino, R. A. Hammond, S. Briand, J. M. Epstein, L. Hébert-Dufresne, and B. M. Althouse. A review and agenda for integrated disease models including social and behavioural factors. *Nat Hum Behav*, 5:834–846, July 2021. URL <https://doi.org/10.1038/s41562-021-01136-2>.
- [7] D. Borukhson, P. Lorenz-Spreen, and M. Ragni. When Does an Individual Accept Misinformation? An Extended Investigation Through Cognitive Modeling. *Comput Brain Behav*, 5(2):244–260, June 2022. URL <https://doi.org/10.1007/s42113-022-00136-3>.
- [8] A. Bovet and H. A. Makse. Influence of fake news in Twitter during the 2016 US presidential election. *Nature communications*, 10(1):7, 2019. URL <https://doi.org/10.1038/s41467-018-07761-2>.
- [9] J. Brainard and P. R. Hunter. Misinformation making a disease outbreak worse: outcomes compared for influenza, monkeypox, and norovirus. *SIMULATION*, 96(4):365–374, Nov. 2019. URL <https://doi.org/10.1177/0037549719885021>.
- [10] D. A. Broniatowski, A. M. Jamison, S. Qi, L. AlKulaib, T. Chen, A. Benton, S. C. Quinn, and M. Dredze. Weaponized health communication: Twitter bots and russian trolls amplify the vaccine debate. *American Journal of Public Health*, 108(10):1378–1384, 2018. doi: 10.2105/AJPH.2018.304567. URL <https://doi.org/10.2105/AJPH.2018.304567>.
- [11] D. A. Broniatowski, J. R. Simons, J. Gu, A. M. Jamison, and L. C. Abrams. The efficacy of Facebook’s vaccine misinformation policies and architecture during the COVID-19 pandemic. *Science Advances*,

- 9(37):eadh2132, 2023. doi: 10.1126/sciadv.adh2132. URL <https://www.science.org/doi/abs/10.1126/sciadv.adh2132>.
- [12] C. Buckee, A. Noor, and L. Sattenspiel. Thinking clearly about social aspects of infectious disease transmission. *Nature*, 595:205–213, July 2021. URL <https://doi.org/10.1038/s41586-021-03694-x>.
- [13] T. Burki. Vaccine misinformation and social media. *The Lancet Digital Health*, 1(6):e258–e259, 2019. URL [https://doi.org/10.1016/S2589-7500\(19\)30136-0](https://doi.org/10.1016/S2589-7500(19)30136-0).
- [14] C. Castellano, S. Fortunato, and V. Loreto. Statistical physics of social dynamics. *Rev. Mod. Phys.*, 81:591–646, 2009. doi: 10.1103/RevModPhys.81.591. URL <https://link.aps.org/doi/10.1103/RevModPhys.81.591>.
- [15] Centers for Disease Control and Prevention. Isolation and Precautions for People with COVID-19, 2023. URL <https://www.cdc.gov/coronavirus/2019-ncov/your-health/isolation.html>. Accessed 2023-06-27.
- [16] D. Centola. The spread of behavior in an online social network experiment. *Science*, 329(5996):1194–1197, 2010.
- [17] H.-W. Chan, C. P.-Y. Chiu, S. Zuo, X. Wang, L. Liu, and Y.-y. Hong. Not-so-straightforward links between believing in COVID-19-related conspiracy theories and engaging in disease-preventive behaviours. *Humanit Soc Sci Commun*, 8(104):1–10, May 2021. URL <https://doi.org/10.1057/s41599-021-00781-2>.
- [18] M. Conover, B. Gonçalves, J. Ratkiewicz, A. Flammini, and F. Menczer. Predicting the political alignment of twitter users. In *Proceedings of 3rd IEEE Conference on Social Computing (SocialCom)*, pages 192–199, 2011. doi: 10.1109/PASSAT/SocialCom.2011.34.
- [19] V. D’Andrea, O. Artime, N. Castaldo, P. Sacco, R. Gallotti, and M. De Domenico. Epidemic proximity and imitation dynamics drive infodemic waves during the COVID-19 pandemic. *Phys Rev Res*, 4(1):013158, Feb. 2022. doi: 10.1103/PhysRevResearch.4.013158. URL <https://doi.org/10.1103/PhysRevResearch.4.013158>.
- [20] V. D’Andrea, R. Gallotti, N. Castaldo, and M. De Domenico. Individual risk perception and empirical social structures shape the dynamics of infectious disease outbreaks. *PLoS Comput Biol*, 18(2): e1009760, Feb. 2022. doi: 10.1371/journal.pcbi.1009760. URL <https://doi.org/10.1371/journal.pcbi.1009760>.
- [21] M. R. DeVerna, F. Pierri, B. T. Truong, J. Bollenbacher, D. Axelrod, N. Loynes, C. Torres-Lugo, K.-C. Yang, F. Menczer, and J. Bryden. CoVaxxy Tweet IDs dataset. Zenodo, Feb. 2021. URL <https://doi.org/10.5281/zenodo.7752586>.

- [22] M. R. DeVerna, F. Pierri, B. T. Truong, J. Bollenbacher, D. Axelrod, N. Loynes, C. Torres-Lugo, K.-C. Yang, F. Menczer, and J. Bryden. CoVaxxy: A Collection of English-Language Twitter Posts About COVID-19 Vaccines. In *Proceedings of the International AAAI Conference on Web and Social Media*, volume 15, pages 992–999, 2021. URL <https://doi.org/10.1609/icwsm.v15i1.18122>.
- [23] M. Di Giovanni, F. Pierri, C. Torres-Lugo, and M. Brambilla. VaccinEU: COVID-19 vaccine conversations on Twitter in French, German and Italian. In *Proceedings of the International AAAI Conference on Web and Social Media*, volume 16, pages 1236–1244, 2022. URL <https://doi.org/10.1609/icwsm.v16i1.19374>.
- [24] M. Dredze, M. J. Paul, S. Bergsma, and H. Tran. Carmen: A twitter geolocation system with applications to public health. In *Proc. AAAI Workshop on Expanding the Boundaries of Health Informatics Using AI (HIAI)*, volume 23, page 45, 2013.
- [25] S. Funk, M. Salathé, and V. A. A. Jansen. Modelling the influence of human behaviour on the spread of infectious diseases: a review. *J R Soc Interface*, 7(50):1247–1256, Sept. 2010. doi: 10.1098/rsif.2010.0142. URL <https://doi.org/10.1098/rsif.2010.0142>.
- [26] R. Gallotti, F. Valle, N. Castaldo, P. Sacco, and M. De Domenico. Assessing the risks of ‘infodemics’ in response to COVID-19 epidemics. *Nature Human Behaviour*, 4(12):1285–1293, 2020. doi: 10.1038/s41562-020-00994-6. URL <https://doi.org/10.1038/s41562-020-00994-6>.
- [27] M. Granovetter. Threshold Models of Collective Behavior. *American Journal of Sociology*, May 1978. URL <https://doi.org/10.1086/226707>.
- [28] N. Grinberg, K. Joseph, L. Friedland, B. Swire-Thompson, and D. Lazer. Fake news on Twitter during the 2016 US presidential election. *Science*, 363(6425):374–378, 2019. URL <https://doi.org/10.1126/science.aau2706>.
- [29] P. Jacob Wallace. Excess Death Rates for Republican and Democratic Registered Voters in Florida and Ohio During the COVID-19. *JAMA Intern Med*, July 2023. URL <https://jamanetwork.com/article.aspx?doi=10.1001/jamainternmed.2023.1154>.
- [30] B. Karrer and M. E. Newman. Stochastic blockmodels and community structure in networks. *Physical Review E*, 83(1):016107, 2011. URL <https://doi.org/10.1103/PhysRevE.83.016107>.
- [31] D. M. Lazer, M. A. Baum, Y. Benkler, A. J. Berinsky, K. M. Greenhill, F. Menczer, M. J. Metzger, B. Nyhan, G. Pennycook, D. Rothschild, et al. The science of fake news. *Science*, 359(6380):1094–1096, 2018. URL <https://doi.org/10.1126/science.aao2998>.
- [32] C. Y. Liu, J. Berlin, M. C. Kiti, E. Del Fava, A. Grow, E. Zagheni, A. Melegaro, S. M. Jenness, S. B. Omer, B. Lopman, and K. Nelson. Rapid Review of Social Contact Patterns During the COVID-19

- Pandemic. *Epidemiology*, 32(6), 2021. doi: 10.1097/EDE.0000000000001412. URL <https://doi.org/10.1097/EDE.0000000000001412>.
- [33] S. Loomba, A. de Figueiredo, S. J. Piatek, K. de Graaf, and H. J. Larson. Measuring the impact of COVID-19 vaccine misinformation on vaccination intent in the UK and USA. *Nature Human Behavior*, 2021. URL <https://doi.org/10.1038/s41562-021-01056-1>.
- [34] T. Mitze, R. Kosfeld, J. Rode, and K. Wälde. Face masks considerably reduce COVID-19 cases in Germany. *Proc Natl Acad Sci U.S.A*, 117(51):32293–32301, Dec. 2020. doi: 10.1073/pnas.2015954117. URL <https://doi.org/10.1073/pnas.2015954117>.
- [35] B. Mønsted, P. Sapieżyński, E. Ferrara, and S. Lehmann. Evidence of complex contagion of information in social media: An experiment using Twitter bots. *PLoS ONE*, 12(9):e0184148, 2017.
- [36] N. Mumtaz, C. Green, and J. Duggan. Exploring the Effect of Misinformation on Infectious Disease Transmission. *Systems*, 10(2):50, Apr. 2022. URL <https://doi.org/10.3390/systems10020050>.
- [37] A. Nematzadeh, E. Ferrara, A. Flammini, and Y.-Y. Ahn. Optimal network modularity for information diffusion. *Phys. Rev. Lett.*, 113:088701, 2014. doi: 10.1103/PhysRevLett.113.088701. URL <https://doi.org/10.1103/PhysRevLett.113.088701>.
- [38] M. Odabaş. 5 facts about Twitter ‘lurkers’. Pew Research Center, 2022. URL <https://www.pewresearch.org/fact-tank/2022/03/16/5-facts-about-twitter-lurkers>.
- [39] F. Pierri, B. L. Perry, M. R. DeVerna, K.-C. Yang, A. Flammini, F. Menczer, and J. Bryden. Online misinformation is linked to early COVID-19 vaccination hesitancy and refusal. *Sci Rep*, 12(5966):1–7, 2022. URL <https://doi.org/10.1038/s41598-022-10070-w>.
- [40] P. Poletti, M. Ajelli, and S. Merler. The effect of risk perception on the 2009 H1N1 pandemic influenza dynamics. *PLOS One*, 6(2):e16460, 2011. URL <https://doi.org/10.1371/journal.pone.0016460>.
- [41] L. Prandi and G. Primiero. Effects of misinformation diffusion during a pandemic. *Appl Network Sci*, 5(1):1–20, Dec. 2020. URL <https://doi.org/10.1007/s41109-020-00327-6>.
- [42] S. Rathje, J. K. He, J. Roozenbeek, J. J. Van Bavel, and S. van der Linden. Social media behavior is associated with vaccine hesitancy. *PNAS Nexus*, 1(4), 2022. URL <https://doi.org/10.1093/pnasnexus/pgac207>.
- [43] R. Robertson. Partisan Bias Scores for Web Domains. Harvard Dataverse, 2018. URL <https://doi.org/10.7910/DVN/QAN5VX>.
- [44] R. E. Robertson, S. Jiang, K. Joseph, L. Friedland, D. Lazer, and C. Wilson. Auditing Partisan Audience Bias within Google Search. *Proc ACM Hum.-Comput Interact*, 2(CSCW):1–22, 2023. URL <https://doi.org/10.1145/3274417>.

- [45] J. Roozenbeek, C. R. Schneider, S. Dryhurst, J. Kerr, A. L. J. Freeman, G. Recchia, A. M. van der Bles, and S. van der Linden. Susceptibility to misinformation about COVID-19 around the world. *R Soc Open Sci*, 7(10):201199, Oct. 2020. URL <https://doi.org/10.1098/rsos.201199>.
- [46] M. Rostila. Birds of a feather flock together — and fall ill? Migrant homophily and health in Sweden. *Sociol Health Illn*, 32(3):382–399, Mar. 2010. URL <https://doi.org/10.1111/j.1467-9566.2009.01196.x>.
- [47] M. Salathé and S. Khandelwal. Assessing Vaccination Sentiments with Online Social Media: Implications for Infectious Disease Dynamics and Control. *PLoS Comput Biol*, 7(10):e1002199, Oct. 2011. doi: <https://doi.org/10.1371/journal.pcbi.1002199>.
- [48] C. Shao, G. L. Ciampaglia, O. Varol, K.-C. Yang, A. Flammini, and F. Menczer. The spread of low-credibility content by social bots. *Nature communications*, 9(1):1–9, 2018. URL <https://doi.org/10.1038/s41467-018-06930-7>.
- [49] K. P. Smith and N. A. Christakis. Social networks and health. *Annu. Rev. Sociol*, 34:405–429, 2008. URL <https://doi.org/10.1146/annurev.soc.34.040507.134601>.
- [50] A. Sontag, T. Rogers, and C. A. Yates. Misinformation can prevent the suppression of epidemics. *J R Soc Interface*, 19(188):20210668, Mar. 2022. URL <https://doi.org/10.1098/rsif.2021.0668>.
- [51] J. Sooknanan and D. M. G. Comissiong. Trending on Social Media: Integrating Social Media into Infectious Disease Dynamics. *Bull Math Biol*, 82(7):1–11, July 2020. URL <https://doi.org/10.1007/s11538-020-00757-4>.
- [52] United States Census Bureau. Population Clock, Nov. 2023. URL <https://www.census.gov/popclock>. [Online; accessed 6. Nov. 2023].
- [53] F. Verelst, L. Willem, and P. Beutels. Behavioural change models for infectious disease transmission: a systematic review (2010-2015). *J R Soc Interface*, 13(125):20160820, 2016. doi: 10.1098/rsif.2016.0820. URL <https://doi.org/10.1098/rsif.2016.0820>.
- [54] L. Weng, F. Menczer, and Y.-Y. Ahn. Virality prediction and community structure in social networks. *Sci. Rep.*, 3(2522), 2013. doi: 10.1038/srep02522. URL <http://dx.doi.org/10.1038/srep02522>.
- [55] Y. Yuan, E. Jahani, S. Zhao, Y.-Y. Ahn, and A. S. Pentland. Implications of COVID-19 vaccination heterogeneity in mobility networks. *Communications Physics*, 6(1):206, 2023.

Supplementary information

1 Mean-field SMIR model

Let us denote the proportions of misinformed and ordinary individuals as μ and $1 - \mu$, respectively. A proportion $\epsilon = 0.001$ of the population is initially infected, split evenly between the ordinary and misinformed groups. Thus, during the initial state, we have initial values for each compartment: $R_O = R_M = 0$, $S_O = \mu - \frac{\epsilon}{2}$, $S_M = 1 - \mu - \frac{\epsilon}{2}$, $I_M = \frac{\epsilon}{2}$, and $I_O = \frac{\epsilon}{2}$.

To identify a suitable base value for the transmission rate among ordinary susceptibles, we begin by exploring the scenario with no misinformed individuals ($\mu = 1$), setting $\gamma = 0.2$ and varying the transmission parameter in the range $0.02 \leq \beta_O \leq 1$. As is typical of SIR dynamics, Fig. S1 shows that lower β_O values delay and lower the infection peak — the so-called “flattening of the curve.” Lower β_O also decreases the total proportion of the population that becomes infected at any point during the epidemic, while higher β_O values increase this proportion. These dynamics are tied to the basic reproduction number $R_0 = \beta/\gamma$: the disease spreading dynamics only reach epidemic levels when $R_0 > 1$, such that an infected individual infects more than one other person on average. This happens when $\beta_O > 0.2$. As R_0 increases, the infection spreads more quickly, the peak infection day occurs sooner, and the proportion of the population that is ultimately infected increases.

We now explore the effect of the recovery rate, again in the scenario with no misinformation or homophily, by setting $\beta_O = 0.3$ and varying the recovery period $\tau = 1/\gamma$ between 1 and 20 days. Fig. S2 shows that when $\tau < 4$, $R_0 < 1$ and the disease does not reach epidemic proportions. At this level, the epidemic takes a long time to reach its peak (≈ 80 days). Increasing τ means that individuals remain infected longer, so the population gets infected faster and the peak infection is reached more rapidly. We set $\tau = 5$ ($\gamma = 0.2$) in the main text to align with quarantine recommendations from the CDC¹⁵. With this value and $\beta_O = 0.3$, the dynamics are at epidemic levels ($R_0 = 1.5$).

2 Robustness analyses

To test the robustness of the main results (Fig. 5C) with respect to the sample size used to construct the contact network, all simulations were rerun after generating contact networks based on the different sampling percentages between 0.01% and 10%. Fig. S3 shows the relative increase in the percentage of the population that becomes infected as a function of the linear threshold ϕ , using the best-case scenario in which the fewest nodes in the network are misinformed as the baseline. We observe a substantial decrease in the effect of misinformation as the sampling size grows to 1%. However, sample sizes above 1% return nearly identical results. We conclude that using a sample size of 10% (as reported in the main text) is sufficient to rule out any size-induced bias.

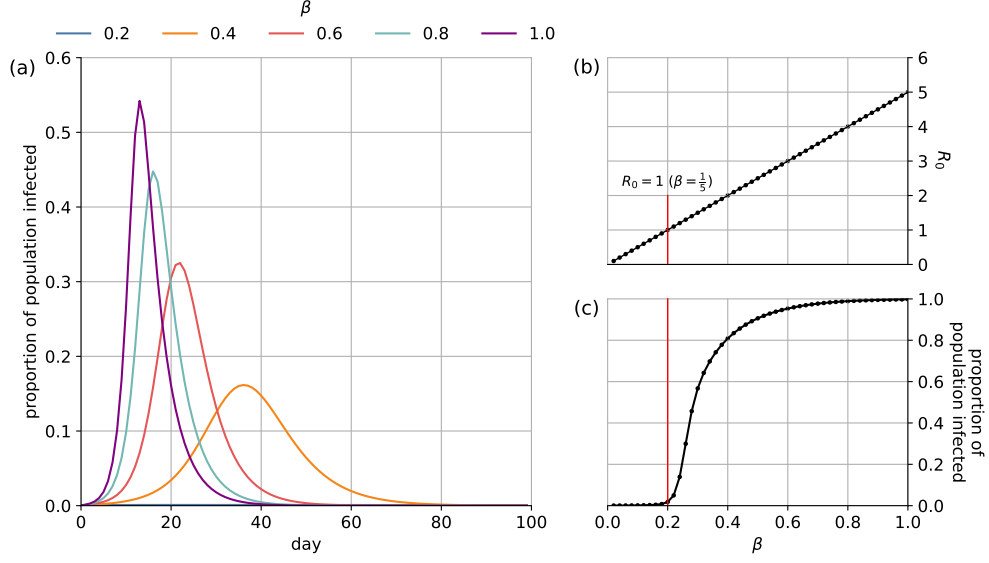


Figure S1: Reducing the transmission parameter β_O decreases the severity of the epidemic. We plot (a) the proportion of the population infected each day, (b) R_0 values, and (c) the total proportion of the population infected as β_O varies. Here we do not consider the role of misinformation or homophily.

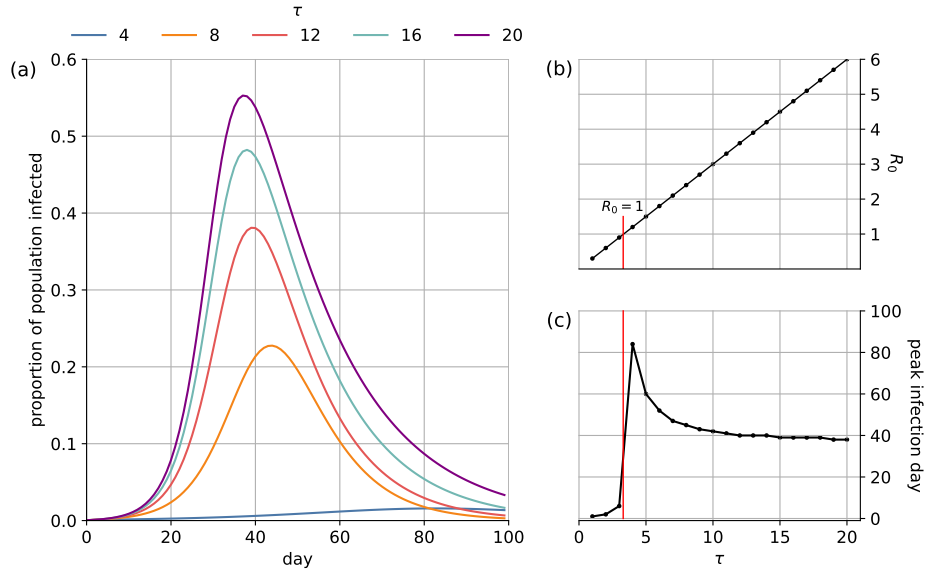


Figure S2: Effects of varying the recovery rate. We plot (a) the proportion of the population infected each day, (b) R_0 values, and (c) the total proportion of the population infected as a function of the number of days to recover, τ . Here we do not consider the role of misinformation or homophily.

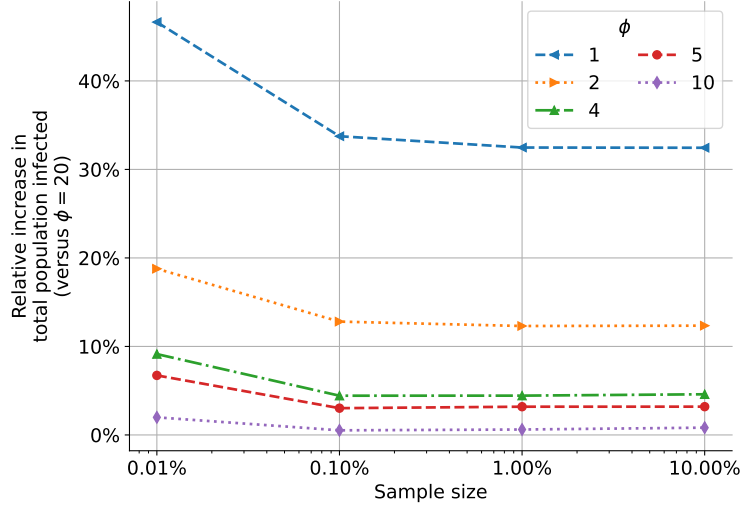


Figure S3: Relative increase in the mean total population infected as a function of the sampling size utilized in the contact network creation process. The $\phi = 20$ scenario, in which the fewest nodes in the network are misinformed, is utilized as the baseline.

We also investigate the impact of the contact network density (\bar{k}) on infection dynamics, as illustrated in Fig. S4 for $5 \leq \bar{k} \leq 25$. We consider this range because $\bar{k} = 25$ represents pre-pandemic daily social contacts while $\bar{k} = 5$ represents COVID-19 lockdown conditions³². As expected, Fig. S4(a) demonstrates that higher \bar{k} leads to increased infections through the population, since the higher contact density provides more opportunities for transmission. But while a larger percentage of the overall population is infected, the relative effect of misinformed individuals decreases. This is because, at higher \bar{k} values, the infected population is already substantial even in the low-misinformation ($\phi = 20$) baseline. The combined effect of these two opposing trends, as shown in Fig. S4(b), is that the additional percentage of infected individuals relative to the $\phi = 20$ scenario reaches a maximum for some intermediate \bar{k} . Fig. S4(b) also shows that, consistent with our primary findings, larger ϕ (misinformed resilience) results in a smaller infected population. In our main analysis we focus on $\bar{k} = 25$ and model an effective reduction of contacts, resulting for example from social distancing or lockdowns, by decreasing the p parameter.

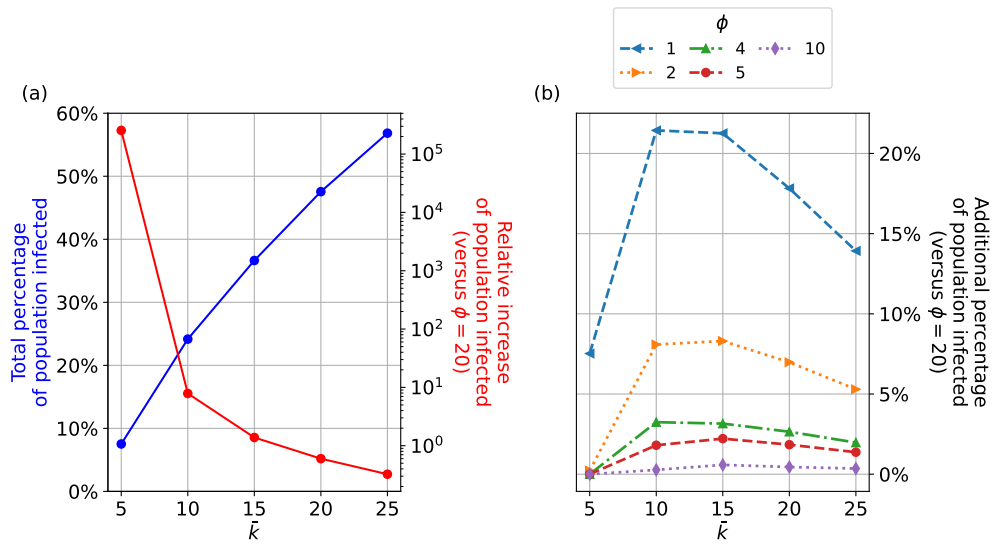


Figure S4: Effects of average contact network degree \bar{k} on infection dynamics. (a) Infected individuals ($\phi = 1$) as a percentage of the overall population and relative to the baseline condition $\phi = 20$, in which the fewest nodes in the network are misinformed. (b) Additional percentages of infected population relative to the baseline condition $\phi = 20$.